Available online at www.sciencedirect.com
ScienceDirect
Bioorganic & Medicinal Chemistry 15 (2007) 800–814
Bioorganic & Medicinal Chemistry

Anti-breast cancer activity of LFM-A13, a potent inhibitor of Polo-like kinase (PLK)

Fatih M. Uckun,* Ilker Dibirdik, Sanjive Qazi, Alexei Vassilev, Hong Ma, Chen Mao, Alexey Benyumov and Katayoon H. Emami†

Paradigm Pharmaceuticals, 2139 4th Street, White Bear Lake, MN 55110, USA
Parker Hughes Cancer Center, St. Paul, MN 55113, USA
CGEN Discovery Inc., 600 Broadway, Suite 580, Seattle, WA 98122, USA

Received 6 July 2006; revised 7 September 2006; accepted 23 October 2006
Available online 26 October 2006

Abstract—Molecular modeling studies led to the identification of LFM-A13 (α-cyano-β-hydroxy-β-methyl-*N*-(2,5-dibromophenyl)propenamide) as a potent inhibitor of Polo-like kinase (Plk). LFM-A13 inhibited recombinant purified Plx1, the *Xenopus* homolog of Plk, in a concentration-dependent fashion, as measured by autophosphorylation and phosphorylation of a substrate Cdc25 peptide. LFM-A13 was a selective Plk inhibitor. While the human PLK3 kinase was also inhibited by LFM-A13 with an IC_{50} value of 61 μM, none of the 7 other serine/threonine kinases, including CDK1, CDK2, CDK3, CHK1, IKK, MAPK1 or SAPK2a, none of the 10 tyrosine kinases, including ABL, BRK, BMX, c-KIT, FYN, IGF1R, PDGFR, JAK2, MET, or YES, or the lipid kinase PI3Kγ were inhibited (IC_{50} values >200–500 μM). The mode of Plk3 inhibition by LFM-A13 was competitive with respect to ATP with a K_i value of 7.2 μM from Dixon plots. LFM-A13 blocked the cell division in a zebrafish (ZF) embryo model at the 16-cell stage of the embryonic development followed by total cell fusion and lysis. LFM-A13 prevented bipolar mitotic spindle assembly in human breast cancer cells and glioblastoma cells and when microinjected into living epithelial cells at the prometaphase stage of cell division, it caused a total mitotic arrest. Notably, LFM-A13-delayed tumor progression in the MMTV/*neu* transgenic mouse model of HER2 positive breast cancer at least as effectively as paclitaxel and gemcitabine. LFM-A13 showed a favorable toxicity profile in mice and rats. In particular there was no evidence of hematologic toxicity as documented by peripheral blood counts and bone marrow examinations. These results establish LFM-A13 as a small molecule inhibitor of Plk with in vitro and in vivo anti-proliferative activity against human breast cancer.

1. Introduction

Mitotic cell cycle progression is tightly regulated through reversible covalent protein phosphorylation events coordinated by regulatory kinases, including members of the Polo subfamily of protein kinases.[1–9] Polo-like kinase (Plk) is a M-phase specific mammalian serine/threonine protein kinase which plays a pivotal role in the activation of the Cdc2-Cyclin B complex/mitosis promoting factor (MPF), maturation and function of centrosomes and spindles, chromosome segregation, initiation of anaphase by regulation of the anaphase-promoting complex (APC), and induction of cytokinesis-associated septal structures.[1–3] The expression pattern and localization of Plk is consistent with its important role in bipolar spindle formation, centrosome maturation, and cytokinesis.[1–3] Plk localizes to the centrosomes, kinetochores, and central spindle structures during mitosis.[1–3] Plk is a highly conserved kinase throughout evolution. It has been shown that Plx1, the Plk homolog from *Xenopus*, phosphorylates and activates Cdc25 tyrosine phosphatase which activates Cdc2.[5–7]

There are several reports of Plk overexpression in cancer cells.[10–19] Plk overexpression is associated with a poor prognosis, especially in breast cancer.[18] Attempts to deplete cancer cells of functional Plk kinase activity using antibody microinjections, antisense RNA, or expression of dominant negative Plk have been shown to result in mitotic catastrophe and apoptotic cell death or induce

Keywords: Polo-like kinase; Mitosis; Transgenic mouse; Cancer.
* Corresponding author. Present address: 2139 4th Street, White Bear Lake, MN 55110, USA. Tel.: +1 651 329 2468; fax: +1 651 653 3262; e-mail: fatih_uckun@ih.org
† Dr. Emami was a fellow of the Leukemia Society of America during parts of this study.

0968-0896/$ - see front matter © 2006 Elsevier Ltd. All rights reserved.
doi:10.1016/j.bmc.2006.10.050

growth inhibition.[19–25] It has been proposed that depletion of Plk kinase activity at the kinetochores of cancer cells may stabilize microtubule attachment to kinetochores and contribute to an imbalance of the spindle checkpoint, causing increased sensitivity to microtubule drugs such as paclitaxel.[19] These results prompted us to search our chemical libraries for potent small molecule inhibitors of Plk as a new class of chemosensitizing anti-proliferative agents against breast cancer.

In a systematic effort to design potent inhibitors of Plk as anti-cancer agents with anti-proliferative and chemosensitizing properties, we have constructed a three-dimensional homology model of the Plk/Plx1 kinase domain (KD). Our modeling studies revealed that the catalytic site of the Plk-KD is composed of a distinct planar rectangular binding region. Of all the compounds evaluated in our modeling studies, we predicted that the rationally designed Bruton's tyrosine kinase (BTK) inhibitor LFM-A13 (α-cyano-β-hydroxy-β-methyl-*N*-(2,5- dibromophenyl)propenamide) would provide the strongest binding to the catalytic site of the Plk-KD. In agreement with this prediction, LFM-A13 bound recombinant purified Plx1, the *Xenopus* homolog of Plk,[6,7,38] as measured by quenching of the intrinsic fluorescence of Plx1, and inhibited its autophosphorylation as well as its phosphorylation of a target Cdc25 peptide in a concentration-dependent fashion. LFM-A13 was a selective Plk inhibitor as it also inhibited PLK3 but none of the 7 other serine/threonine kinases, including CDK1, CDK2, CDK3, CHK1, IKK, MAPK1 or SAPK2a, none of the 10 tyrosine kinases, including ABL, BRK, BMX, c-KIT, FYN, IGF1R, PDGFR, JAK2, MET, or YES, or the lipid kinase PI3Kγ (IC_{50} values >200–500 μM). The anti-proliferative activity of LFM-A13 was examined in a zebrafish (ZF) embryo model. LFM-A13 blocked the cell division at the 16-cell stage of the embryonic development followed by total cell fusion and lysis. When microinjected into living PTK1 epithelial cells at the prometaphase stage of cell division, LFM-A13 caused a total mitotic arrest. LFM-A13 prevented bipolar mitotic spindle assembly in human breast cancer cells as well as human brain tumor/glioblastoma cells, as determined by confocal laser scanning microscopy. Notably, LFM-A13 delayed tumor progression in the MMTV/*Neu* transgenic mouse model of HER2 positive breast cancer at least as effectively as paclitaxel or gemcitabine. These results indicate that LFM-A13 may be useful as a potent Plk inhibitor in the treatment of breast cancer patients.

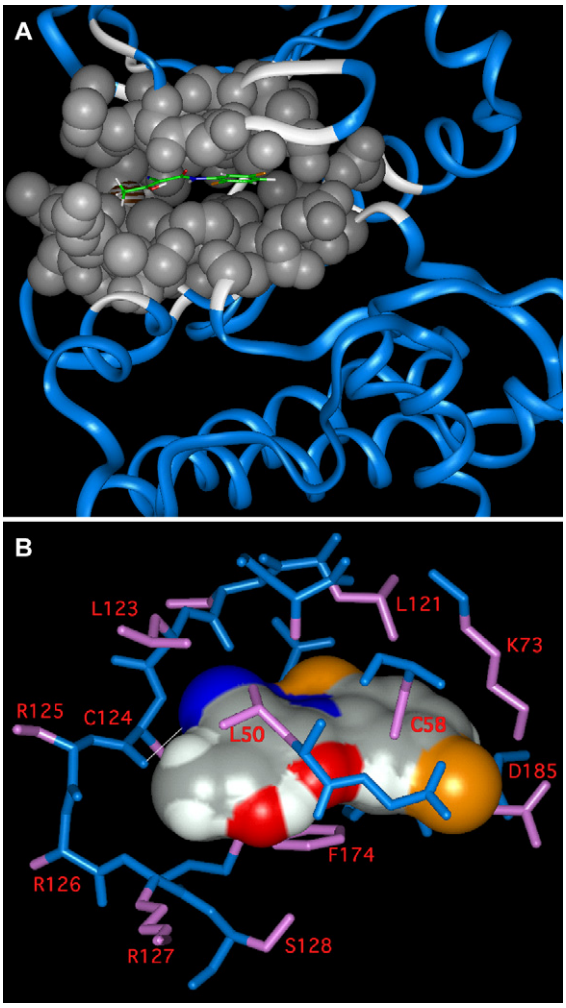

Figure 1. (A) Homology model of Plx1-KD with LFM-A13 that was docked into the ATP binding site. Plx1-KD is shown in ribbon representation and LFM-A13 in a stick model. The non-hydrogen residues that are close to the ligand within 7 Å are shown in a white space-filling model. (B) A close-up view of the Plx1-KD binding site and LFM-A13 (spacing-filling model). The side chains of the binding site residues are shown in blue and the main chains in pink. The amide NH of residue C124 on a linker region that connected the N-lobe with the C-lobe is hydrogen bound to the cyano group of LFM-A13 and the hydrogen bond is illustrated as a white line.

2. Results

2.1. Molecular modeling studies identify LFM-A13 as a candidate Plk inhibitor

The structural homology model of the PLK/Plx1 kinase domain (PLK/Plx1-KD) is shown in Figure 1. Plx1-KD has a two-lobe fold reminiscent of the topology of other PTK kinase domain structures. The N-terminal lobe (residues 38–289) contains five strands of anti-parallel β sheets (b1–b5) and one α-helix (C helix). The C-terminal lobe (residues 126–289) contains a 4-helix bundle (αD, αE, αF, and αH) flanked by a short antiparallelled β sheet (b6, b8 and b9) and four additional helices (αI, αDE, αEF, and αHI). The N- and C-lobes are connected by a linker region (residues 122-126) and form a cleft at the ATP binding site.

The overall architecture of the Plx1-KD revealed that the catalytic site is composed of a distinct planar rectangular binding region defined by residues from Leu-121, Arg-125, Asp-185, and Lys-169, which occupy the corners of the rectangle. The far left corner of the rectangle can be visualized as beginning close to the hinge region at Leu-121 and extending 8 Å toward the upper right to Asp-185. This is the shortest side of the binding pocket and is located closer to the protein core. The left side of the pocket extends from Leu-121 and traces 12 Å along

the hinge region up to Arg-125. The right side of the rectangular pocket, opposite to the hinge region, extends approximately 16 Å from Asp-185 to Lys-169, which is immediately adjacent to the binding subsites for the sugar and triphosphate groups of ATP. The hinge region of the binding site is composed of residues 122–126. The solvent-exposed and fourth side of the rectangle extends 18 Å along the slot-shaped opening from Arg-125 to Lys-169. The binding pocket is wider at the opening toward solvent; it narrows toward the innermost region of the binding site, and overall it is relatively shallow with a thickness of about 7 Å.

In modeling studies, members of a leflunomide metabolite analog (LFM-A) compound library were docked into the Plx1-KD catalytic site such that they would be positioned along the hinge region, corresponding to a quite common position that a protein kinase inhibitor would take to ensure a hydrogen bond with the hinge region according to observation in many crystal structures of kinase/inhibitor complexes. Our docking studies predicted that compound LFM-A13 would fit into the catalytic site of Plx1-KD best and provide the strongest binding. The positions of the critical residues in the active site of the Plx1-KD and the docked position of the lead compound LFM-A13 are shown in Figure 1. Of all the possible orientations of this molecule bound to the catalytic site, the one shown in Figure 1A and B provided the highest interaction score (K_i = 15 μM) with Plx1-KD indicative of an energetically favored binding mode. The energetically favorable position of LFM-A13 in the catalytic site is such that LFM-A13 molecule is sandwiched between two regions of mostly hydrophobic residues (Fig. 1B). The region above the docked inhibitor near the glycine-rich ATP binding loop (residues 49–59) consisted of residues Leu-50, Ala-71, and Cys-58 including the backbone of the ATP-binding-loop, and the residues below the docked inhibitor including Plx1-KD residues Phe-174 and Cys-124 (Fig. 1B).

2.2. LFM-A13 binds to and inhibits purified recombinant Plx1

Recombinant Plx1 was expressed in a baculovirus vector expression system using Sf21 cells and purified for in vitro fluorescence quenching experiments and kinase assays (Fig. 2A). Our docking studies predicted that LFM-A13 strongly binds the catalytic site of Plx1-KD. This prediction was confirmed in tryptophan (Trp)-associated intrinsic fluorescence quenching experiments. The intrinsic fluorescence of Plx1 displayed a marked and concentration-dependent quenching in the presence of LFM-A13 indicative of conformational changes in Plx1 protein induced by LFM-A13 binding. The quenching curve showed saturation at higher concentrations of LFM-A13 with an estimated K_d value of 15 ± 2 μM (Fig. 2B). Strong quenching of the Trp fluorescence may be attributed to highly efficient energy transfer to the drug molecule from Trp residues close to the binding site, or to a direct interaction (static quenching) since there is practically no overlap between the emission spectrum of Trp and the absorption spectrum of LFM-A13. Quenching in this case may be speculated to arise from either a direct interaction of the Br atom(s) in LFM-A13 with Trp residues in protein, or possibly a conformational change.

In order to obtain a physiologically active Plx1, we treated the infected Sf21 cells with okadaic acid for 3 h prior to the harvest time to promote entry into mitosis as has been reported previously.[7] Okadaic acid inhibits the activity of phosphatases like PP2A and would drive the cells into a state resembling mitosis. LFM-A13 was effective as a kinase inhibitor against the purified mitotic form of recombinant Plx1. The kinase activity of Plx1, as measured by autophosphorylation, was inhibited by LFM-A13 with an IC_{50} value of 3.7 μg/mL (=10.3 μM) (Fig. 3A and B). The kinase activity of Plx1, as measured by phosphorylation of GST-Cdc25, which was used as an exogenous kinase substrate (Fig. 3C and D), was inhibited by micromolar concentrations of LFM-A13 in a concentration-dependent fashion with an IC_{50} value of 11.7 μg/mL (=32.5 μM). Immunoblotting using anti-Plk antibodies (Fig. 3B) and anti-Cdc25 antibodies (Fig. 3D) confirmed that approximately equal amounts of Plx1 protein and GST-Cdc25 were present in each reaction mixture. Therefore, the observed reduction in autophosphorylation or substrate phosphorylation at increasing LFM-A13 concentrations was not owing to a significantly lower Plx protein content or substrate content in these reaction mixtures.

As shown in Table 1, LFM-A13 was a selective Plk inhibitor. While the human PLK3 kinase was also inhibited by LFM-A13 with an IC_{50} value of 61 μM, none of the 7 other serine/threonine kinases, including CDK1, CDK2, CDK3, CHK1, IKK, MAPK1 or SAPK2a, none of the 10 tyrosine kinases, including ABL, BRK, BMX, c-KIT, FYN, IGF1R, PDGFR, JAK2, MET, or YES, or the lipid kinase PI3Kγ were inhibited (IC_{50} values >200–500 μM).

We next sought to determine the mode of LFM-A13-induced inhibition of human PLK3. Titration experiments using 5 different concentrations of ATP revealed a competitive inhibition of PLK3 by LFM-A13 with respect to ATP. Kinase activity was inhibited by LFM-A13 at each of the 5 ATP concentrations (25, 50, 75, 100, 200 μM). At each ATP concentration, the IC_{50} value was calculated by fitting the inhibition curves to the dose effect equation by method of least squares: % inhibition = $(100 \times [\text{LFM-A13}])/IC_{50}/(100 + [\text{LFM-A13}]/IC_{50})$. The IC_{50} values were 61 μM at 25 μM ATP, 79 μM at 50 μM ATP, 120 μM at 75 μM ATP, 125 μM at 100 μM ATP, and 262 μM at 200 μM ATP (Fig. 4A). A K_i value of 25 μM was determined from the intercept of the plot of [ATP] versus IC_{50} values ($IC_{50} = K_i/K_m^X[\text{ATP}] + K_i$) (Fig. 4A). The K_i of PLK3 by LFM-A13 was also calculated by the point of linear intersection from the Dixon plots of the intensity of phosphorylation of substrate ($1/v$) vs the concentration of the LFM-A13 as the inhibitor (i), and found to be equal to 7.2 μM (Fig. 4B). In summary, LFM-A13 exhibited a competitive mode of inhibition against PLK3.

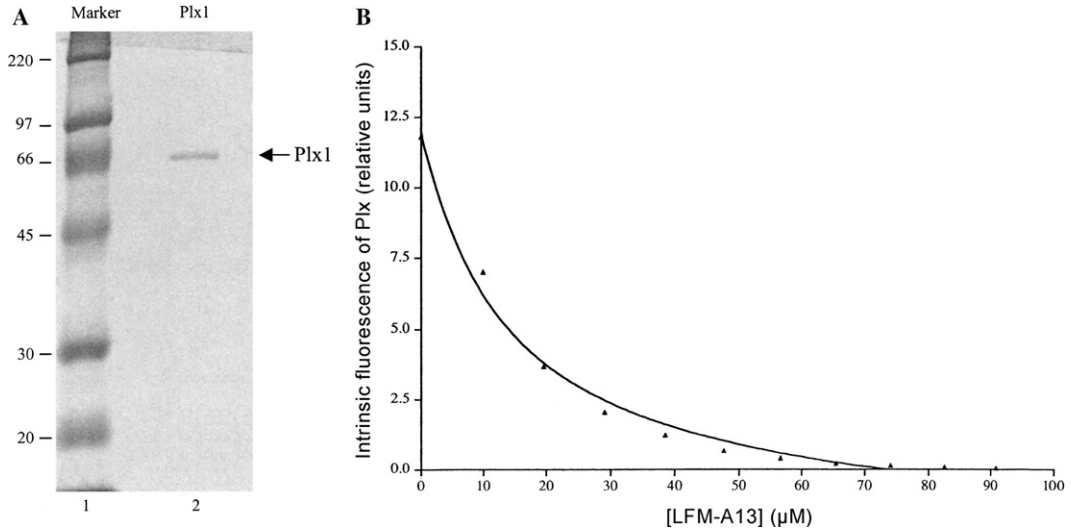

Figure 2. (A) Purified recombinant His6-Plx1 protein. Histidine-tagged recombinant Plx protein was purified as previously reported. The purified protein was visualized by Coomassie blue staining. (B) Quenching of Plx1 intrinsic fluorescence in the presence of LFM-A13. The quenching curve shows saturation and demonstrates that the intrinsic fluorescence of Plx is modulated by the binding of LFM-A13. The K_d value estimated from fitting the data to an equation describing binding to a single type of site was of 15 ± 2 μM.

2.3. In vitro anti-proliferative activity of LFM-A13

The antiproliferative activity of LFM-A13 was examined in a zebrafish embryo model. At a constant temperature of 28.5 °C (ST), the ZF egg cleaves first at 45 min post fertilization forming the two-cell stage egg. Untreated or sham-treated two-cell stage zebrafish embryos reach 4-cell, 8-cell, and 64-cell stages within 15 min, 30 min, and 75 min, respectively.[26,27] Within 3.5 h post-fertilization, the zebrafish embryo develops into a high blastula and undergoes gastrulation 2 h later.[26,27] LFM-A13 blocked the cell division at the 16-cell stage of the embryonic development followed by total cell fusion and lysis. When the two-cell stage zebrafish eggs were treated with LFM-A13 (500 μM, water-borne administration), they developed normally for 30-35 min, up to the 8-16-cell stage, and then at the 16-cell stage they showed a proliferation arrest followed by cell fusion and lysis (Fig. 5). Snapshots of the LFM-A13-treated eggs were taken at the 8- to 16-cell stage after 35 min of exposure (Fig. 5B), 45 min of exposure (Fig. 5D), and 60 min of exposure (Fig. 5F). At 35 min, unlike the sham-treated (vehicle: 2.5% DMSO) control eggs (Fig. 5A), LFM-A13-treated eggs showed deterioration of cell division and cell disorientation, and initial signs of cell fusion (Fig. 5B). Within the next 10 min, cell fusion dramatically progressed in LFM-A13-treated eggs (Fig. 5D), while control eggs continued the cell division without any apparent delay (Fig. 5C). Eggs treated with LFM-A13 for 60 min showed total cell fusion and lysis (Fig. 5F), whereas no alteration in cell division and development was observed in sham-treated control eggs (Fig. 5E). Thus, LFM-A13 blocked the cell division in a zebrafish embryo model at the 16-cell stage of the embryonic development followed by total cell fusion and lysis. Cell division blockade and developmental arrest caused by LFM-A13 were irreversible.

We next examined the anti-proliferative effects of LFM-A13 by microinjecting it into PTK1 cells at pre-mitotic stages of the cell cycle and monitoring cell cycle progression post-injection. Control PTK1 cells at the prometaphase stage of the cell cycle microinjected with a 10% DMSO solution progressed from prometaphase to cytokinesis within 30 min (Fig. 6A). In contrast, when prometaphase cells were injected with a 1 mM LFM-A13 solution in 10% DMSO, they showed a complete arrest with no signs of cell cycle progression within the 50 min of monitoring period (Fig. 6B). We also studied the effects of LFM-A13 on progression of PTK1 cells from anaphase to cytokinesis. Microinjection of LFM-A13 into anaphase cells resulted in a significant delay in completion of mitosis (Fig. 6C).

Plk plays a pivotal role in the organization of the spindles during mitosis. This is essential for the proper segregation and alignment of chromosomes.[3] Confocal laser scanning microscopy experiments demonstrated that LFM-A13 prevents the normal process of microtubule assembly as reflected by a very low mitotic index (<0.5%) and gross mitotic aberrations. Specifically, LFM-A13 induced aberrant monopolar or multipolar (instead of normal bipolar) spindle formation in human BT20 breast cancer cells (Fig. 7A and B). The spindle microtubules appeared abnormally dense and long extending to cell margins. Similar results were obtained using U373 glioblastoma cells as targets (Fig. 7C–F). No immediate apoptotic changes were apparent in breast cancer or glioblastoma cells when examined by confocal microscopy after 2 h of treatment with LFM-A13 (Fig. 7). These effects of LFM-A13 are consistent with the known function of Plk in promotion of cytokinesis and formation as well as positioning of the central spindle.[3]

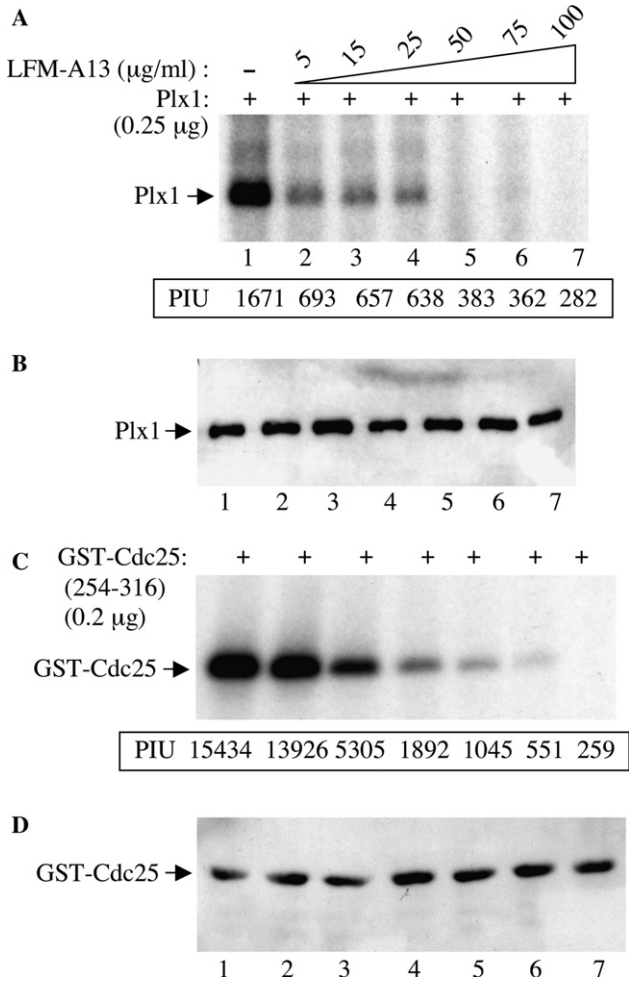

Figure 3. LFM-A13 is a potent inhibitor of Plk kinase activity. (A) A highly purified preparation of Plx1 (250 ng/kinase reaction) produced in a baculovirus vector expression system was treated for 1 h at room temperature with LFM-A13 at the indicated concentrations. The enzymatic activity of Plx1 was determined by measuring autophosphorylation in a 15-min kinase assay. PIU: Phosphorimager units. (B) A parallel kinase assay was performed in the presence of cold ATP and Western blot analysis was performed to compare the amount of Plx-1 protein in each kinase reaction sample. (C) The enzymatic activity of Plx1 was measured in a kinase reaction using recombinant GST-Cdc25 (200 ng/kinase reaction) as an exogenous substrate in the absence (lane 1) and presence of increasing concentrations of LFM-A13 (lanes 2–7). PIU: Phosphorimager units. (D) Western blot analysis was performed to compare the amount of substrate in each kinase reaction sample.

2.4. Toxicity of LFM-A13 in mice and rats

In previous studies, we found that LFM-A13 did not affect the viability of normal or leukemic lymphohematopoietic cell lines.[30,39] Therefore, we hypothesized that LFM-A13 would not cause hematologic toxicity in animals. In order to test this hypothesis, we examined the effects of LFM-A13 on peripheral blood counts as well as cellularity and cellular composition of bone marrows in CD-1 mice, BALB/c mice, and Lewis rats. As shown in Tables 2 and 3, no hematologic toxicity was observed in LFM-A13 treated rodents at dose levels as high as 200 mg/kg or cumulative dose levels as high as 11.2 g/kg. No significant differences were observed between vehicle-treated control mice or rats and LFM-A13-treated test mice or rats relative to their post-treatment WBC, ANC, and ALC values. No myeloid or lymphoid hypoplasia was encountered in the bone marrows of any of the LFM-A13-treated mice or rats (Tables 2 and 3).

LFM-A13, when administered as a single i.p. bolus injection, did not cause severe toxicity in CD-1 mice ($N = 160$) that was associated with morbidity or mortality at dose levels ranging from 10 mg/kg to 80 mg/kg (Table 4). The LD_{10} (i.e., the dose level associated with 10% lethality) was >80 mg/kg. Histopathologic examination of multiple tissues from these mice revealed no lesions in non-proliferating tissues, including the myocardium, kidney, pancreas, lungs, and brain.

LFM-A13, when administered as a single oral bolus dose via gavage in a suspension formulation, did not cause severe toxicity in mice ($N = 75$) that was associated with morbidity or mortality at 25–100 mg/kg dose levels (Table 1). The LD_{10} was >100 mg/kg. Histopathologic examination of multiple tissues from LFM-A13-treated mice did not reveal any test article related toxic lesions. Similarly, when LFM-A13 was administered daily via oral gavage in a suspension formulation for 7–56 consecutive days, it did not cause severe toxicity in mice ($N = 80$) that was associated with morbidity or mortality at dose levels ranging from 25 mg/kg to 200 mg/kg (Table 4). The LD_{10} was >200 mg/kg/day or 11.2 g/kg/treatment course. Histopathologic examination of multiple tissues from LFM-A13-treated mice did not reveal any test article related toxic lesions. LFM-A13, when administered as a single i.v. bolus injection, did not cause severe toxicity in Lewis rats ($n = 30$) that was associated with morbidity or mortality at dose levels ranging from 20 mg/kg to 80 mg/kg (Table 4). The LD_{10} was >80 mg/kg. Histopathologic examination of multiple tissues from LFM-A13-treated rats did not reveal any test article related toxic lesions. Taken together this favorable toxicity profile shows that, at the indicated dose levels, LFM-A13 does not cause detectable damage to the hematopoietic cells or non-hematopoietic tissues in the various organs of mice and rats.

2.5. Anti-breast cancer activity of compound LFM-A13 in MMTV/*Neu* transgenic mice

In MMTV/*Neu* transgenic mice, the wild-type *neu* gene is overexpressed in the mammary gland under the control of the MMTV long terminal repeat. *Neu* transgenic mice invariably develop rapidly progressive and metastatic breast cancer.[26] This animal model has been used to evaluate the anti-proliferative activity of LFM-A13 against Her2/*Neu* overexpressing breast cancer. In vehicle-treated control mice, the size of target tumors ($N = 10$) with a starting average volume of 293 ± 61 mm^3 was tripled within 2 weeks (Fig. 8A). By 3 weeks, the tumors were 3.9 ± 0.6 times larger than the original average tumor size at the start of the experiment (Fig. 8B). The MANOVA model explained a significant portion of the variation ($F_{9,30} = 5.03$, $p = 0.0004$) of the tumor progression measured at 7, 14, and 21 days. There was a significant treat-

Table 1. Selectivity of LFM-A13 as a Plk inhibitor

Target kinases	IC_{50} (μM)
(A) Serine/threonine kinases	
Cyclin-dependent kinase 1 (CDK1)	>500
Cyclin-dependent kinase 2 (CDK2)	>500
Cyclin-dependent kinase 3 (CDK3)	>500
Checkpoint kinase 1 (CHK1)	>500
IκB kinase (IKK)	>500
Mitogen-activated protein kinase 1 (MAPK1)	>500
Plx1	10
Polo-like kinase 3 (PLK3)	61
Stress-activated protein kinase 2a (SAPK2a)	>500
(B) Tyrosine kinases	
Abelson tyrosine kinase (ABL)	>500
Breast tumor kinase (BRK)	267
Bmx kinase (BMX)	281
C-Kit receptor kinase (C-Kit)	>500
Fyn tyrosine kinase (FYN)	240
Insulin-like growth factor 1 receptor kinase (IGF1R)	>500
Janus kinase 2 (JAK2)	>500
Hepatocyte growth factor receptor kinase (Met)	215
Platelet-derived growth factor receptor kinase (PDGFR)	>500
Yes tyrosine kinase (YES)	>500
(C) Lipid kinases	
Phosphatidylinositol 3 kinase γ (Pl3Kγ)	>500

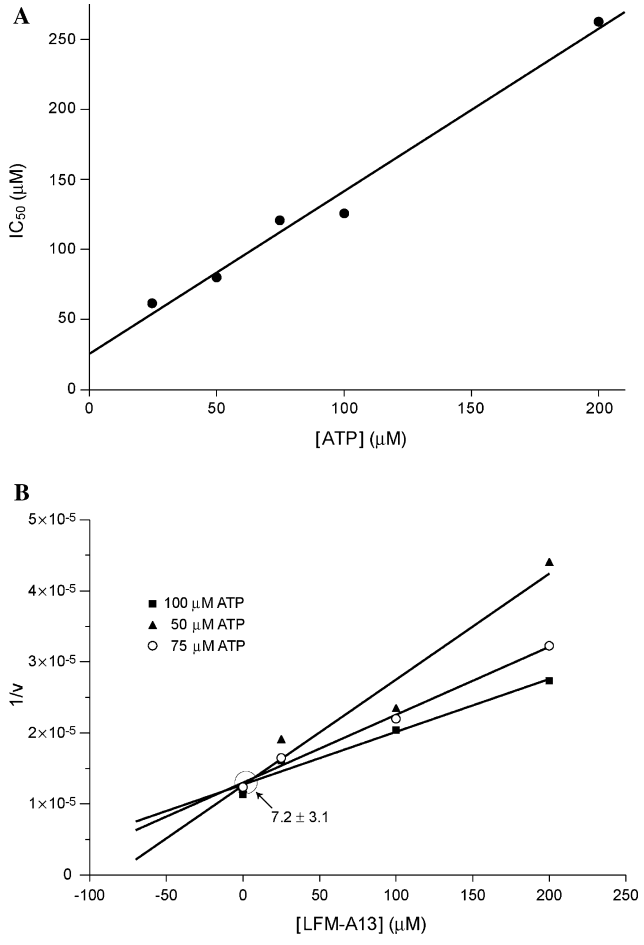

Figure 4. Inhibition of human Plk3 by LFM-A13. (A) ATP-concentration-dependent IC_{50} values of LFM-A13 against Plk3. (B) Dixon plots of Plk3 inhibition by LFM-A13 at 3 different ATP concentrations.

ment effect across the three time points ($F_{4,30} = 2.7$, $p = 0.049$). The normalized tumor volumes were highly correlated with the starting volumes ($F_{1,30} = 11.8$, $p = 0.002$) and the significant interaction term suggested that across all three time points the treatment effect was dependent on the starting volume ($F_{4,30} = 2.8$, $p = 0.046$). The ANCOVA model used to dissect the treatment effects at specific time points, taking into account the effect of starting tumor volumes on tumor progression, showed significant effects at 14 ($F_{4,36} = 2.8$, $p = 0.04$) and 21 days ($F_{4,37} = 4.7$, $p = 0.004$). Interaction terms at 14 days ($p = 0.27$) and 21 days ($p = 0.10$) were not significant suggesting the drug effect was not dependent on the starting volume of the tumor at these time points. Linear contrasts on log transformed values of tumor volumes performed at 21 days showed that tumor progression was significantly delayed by 50 mg/kg LFM-A13 ($P = 0.04$) relative to vehicle control. At 21 days, the average volume of target tumors ($N = 7$) was only 1.8 ± 0.4 times larger than the original average tumor volume. At this dose level, LFM-A13 was at least as effective as paclitaxel or gemcitabine at the clinically applicable dose levels (Fig. 8B). By comparison, target tumors of *neu* transgenic mice treated with 10 mg/kg LFM-A13 ($N = 23$) showed a rapid growth which was as fast as in vehicle-treated control mice (Fig. 8). We compared the results obtained with paclitaxel, gemcitabine, and 50 mg/kg LFM-A13 to the combined data from vehicle and 10 mg/kg LFM-A13 treatment groups. *Neu* transgenic mice treated with 50 mg/kg LFM-A13 had a significantly slower tumor growth rate than mice treated with vehicle or 10 mg/kg LFM-A13 ($P = 0.0036$). There was a trend toward a slower tumor growth rate in transgenic mice treated with paclitaxel ($P = 0.08$) or gemcitabine ($P = 0.10$) when compared to mice vehicle or 10 mg/kg LFM-A13. While the combined group of mice treated with gemcitabine or paclitaxel exhibited a tumor growth rate that was slower than the tumor growth rate in mice treated with vehicle or 10 mg/kg LFM-A13 ($P = 0.034$), their tumor growth rate was not different from the tumor growth rate of mice treated with 50 mg/kg LFM-A13 ($P = 0.14$). The results obtained with gemcitabine were very similar to those achieved with 50 mg/kg LFM-A13 ($P = 0.21$). Taken together, the results demonstrate that LFM-A13 has dose-dependent in vivo anti-cancer activity in the MMTV/*Neu* transgenic mouse model of breast cancer.

3. Discussion

Polo-like kinase (Plk) has recently emerged as a potential anti-cancer drug target candidate for breast cancer, prostate cancer, and stomach cancer.[10–19] Partial depletion of cancer cells of functional Plk kinase activity has been shown to trigger apoptotic cell death or induce growth inhibition.[19–25] In a systematic effort to identify potent inhibitors of Plk as anti-cancer agents, we have constructed a three-dimensional homology model of the Plk kinase domain. Our modeling studies allowed us to identify LFM-A13 as a potential Plk inhibitor. The predictions of the modeling studies were confirmed biochemically by showing that LFM-A13 inhibits the

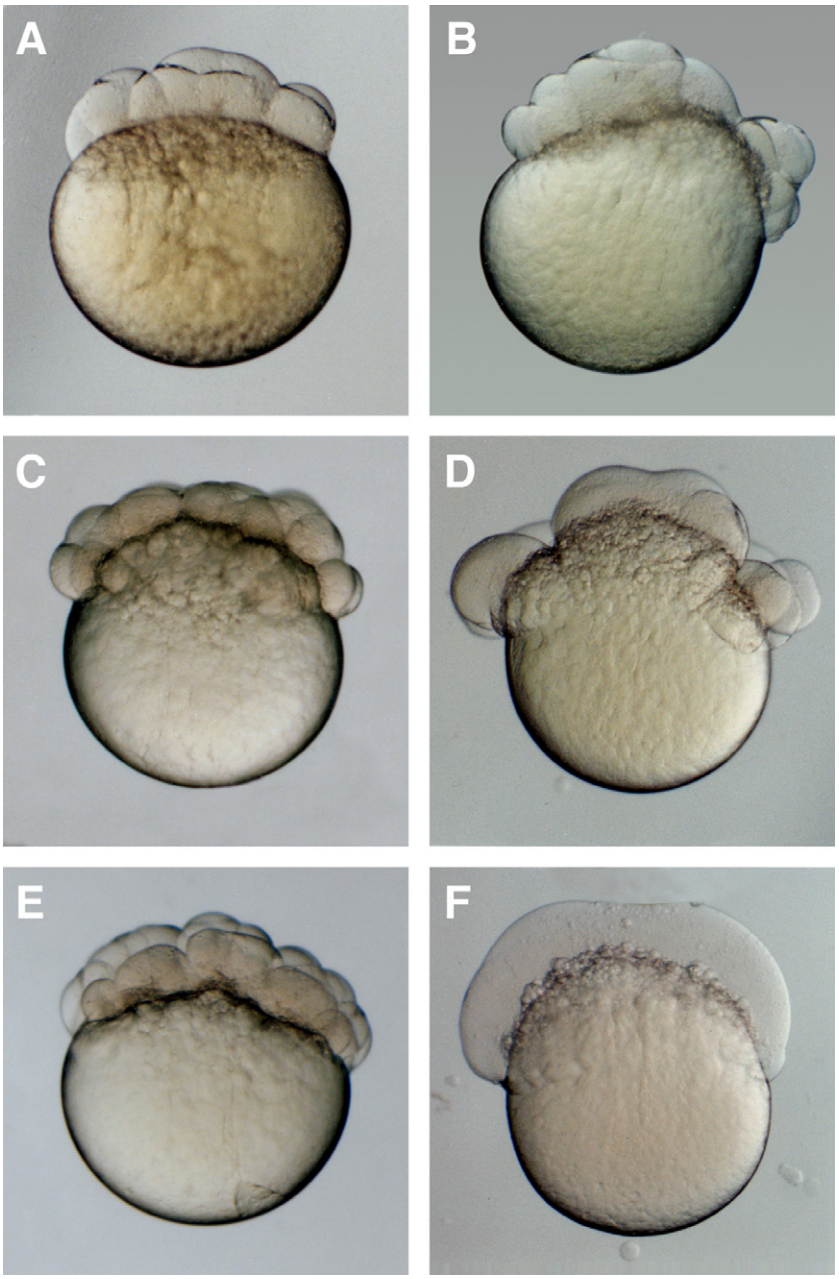

Figure 5. Effect of LFM-A13 on cell division and development in the zebrafish embryo. (A and B) Zebrafish eggs after 35 min of exposure to vehicle (A) or LFM-A13 (B). (C and D) Zebrafish eggs after 45 min of exposure to vehicle (C) or LFM-A13 (D). (E and F) Zebrafish eggs after 60 min of exposure to vehicle (E) or LFM-A13 (F). For the first 30 min, the eggs proceeded with no visible alterations from the 2-cell stage to the 4-cell and then 8-cell stages (not shown). At 35 min, the transition to the 16-cell stage was normal in sham-treated eggs (A) but deteriorated in LFM-A13-treated eggs. At 45 min, sham-treated eggs developed through the 16-cell stage (C) whereas LFM-A13-treated eggs showed cell division blockade, cell fusion, and developmental arrest. At 60 min of exposure, sham-treated eggs reached the 32-cell stage (E) whereas the LFM-A13-treated eggs displayed total cell fusion and lysis (F).

in vitro kinase activity of recombinant Plx1, the *Xenopus* homolog of Plk, as well as recombinant human Plk3 at micromolar concentrations. LFM-13 exhibited a competitive mode of inhibition against Plk3 with a K_i value of 7.2 μM.

We next sought out to determine if LFM-A13 exhibits anti-proliferative activity consistent with its ability to inhibit Plk kinase. LFM-A13 blocked the cell division in a zebrafish embryo model at the 16-cell stage of the embryonic development followed by total cell fusion and lysis, and it prevented bipolar mitotic spindle assembly in human breast cancer cells as well as glioblastoma cells. Notably, LFM-A13 delayed tumor progression in the MMTV/*Neu* transgenic mouse model of HER2 positive breast cancer as effectively as paclitaxel and gemcitabine. LFM-A13 showed a favorable toxicity profile in mice and rats. At single daily dose levels as high as 100–200 mg/day or cumulative dose levels as high as 11.2 g/kg, LFM-A13 did not cause detectable

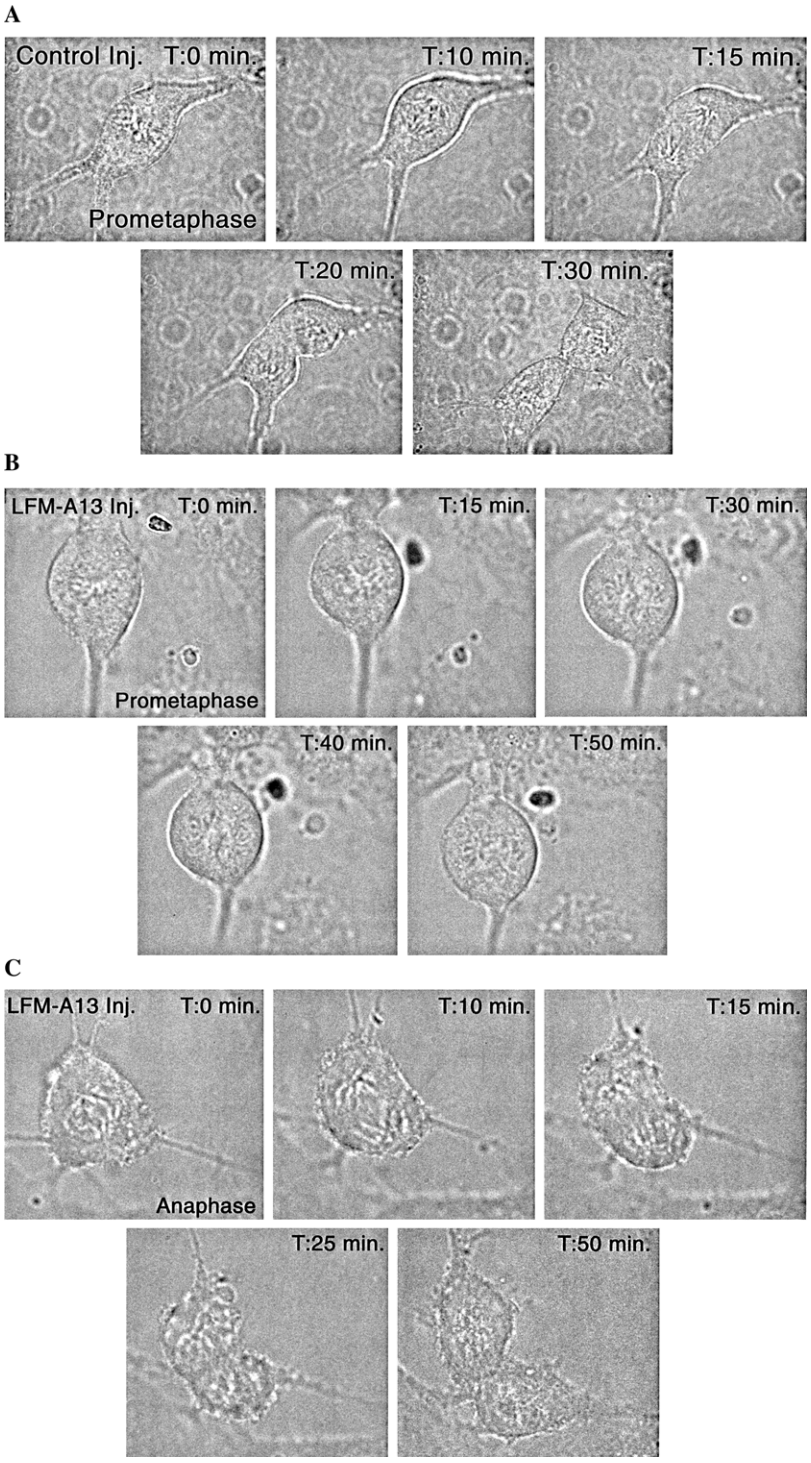

Figure 6. Microinjection and time-lapse imaging. Randomly selected premitotic PTK1 cells were microinjected with 100 μM LFM-A13 using an Eppendorf system (Transjector 5246) under an inverted phase microscope. Cells were imaged for an hour in 1-min intervals using a Nikon Diaphot 200 inverted phase microscope mounted with a stage-top incubator in which the temperature was kept at 37 °C. Digital images were saved using the Metamorph 4.0 software (Universal Imaging Corp) and later processed with Adobe Photoshop software (Adobe Systems, Mountain View, CA). (A) Time-lapse imaging of prometaphase PTK1 cells injected with Vehicle. (B) Time-lapse imaging of prometaphase PTK1 cells injected with LFM-A13. (C) Time-lapse imaging of anaphase PTK1 cells injected with LFM-A13.

damage to the hematopoietic cells or non-hematopoietic tissues in the various organs of mice and rats. These results indicate that LFM-A13 may be useful as a potent Plk inhibitor in the treatment of breast cancer patients.

LFM-A13 is a dual-function kinase inhibitor of BTK tyrosine kinase and Plk serine/threonine kinase activity. LFM-A13 was first developed as an inhibitor of Bruton's tyrosine kinase (BTK) and the first anti-leukemic agent targeting BTK.[39] BTK selectivity of LFM-A13

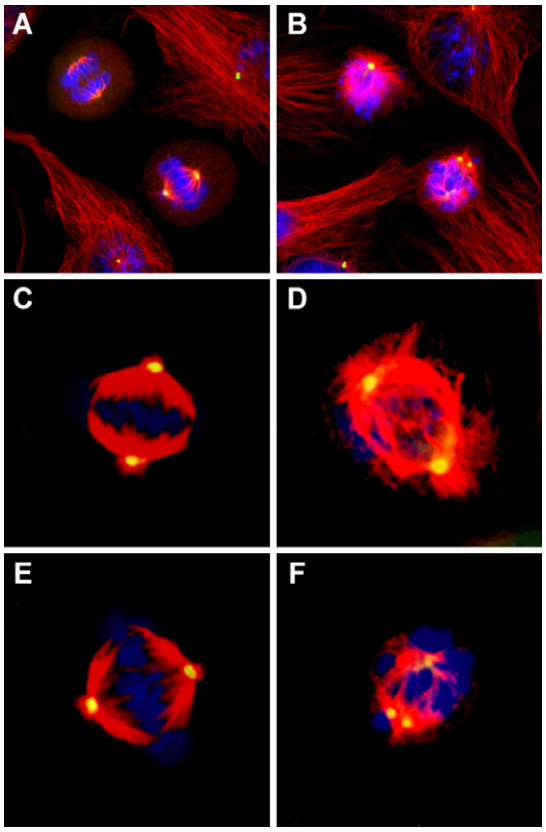

Figure 7. Effects of LFM-A13 on bipolar spindle assembly in BT20 human breast cancer cells and U373 human glioblastoma cells. Confocal laser scanning microscopy experiments demonstrated that LFM-A13 (100 μM) prevents the normal process of microtubule assembly and induces aberrant multipolar or monopolar (instead of normal bipolar) spindle formation in BT20 breast cancer cells and U373 glioblastoma cells. (A) Bipolar mitotic spindles in vehicle-treated BT20 cells as assessed by the presence of α-tubulin (red) and spindle-associated γ-tubulin (green-yellow). Chromosomes (blue) are aligned on the metaphase plate. (B) Aberrant monopolar and multipolar spindles in LFM-A13 treated BT20 cells. (C and E) Bipolar mitotic spindles in vehicle-treated U373 cells as assessed by the presence of α-tubulin (red) and spindle-associated γ-tubulin (green-yellow). Chromosomes (blue) are aligned on the metaphase plate. (D and F) Aberrant bipolar and multipolar spindles in LFM-A13 treated U373 cells.

was confirmed by Kim et al. who showed that, in human Burkitt's leukemia/lymphoma cell line RAMOS, LFM-A13 causes 70% inhibition of BTK-dependent specific phosphorylation of the BTK substrate phospholipase C gamma 2 (PLC-γ2) on Y753 and Y759 residues without affecting Y1217 phosphorylation and its effects are virtually identical to those of BTK-specific short interfering RNA duplexes (siRNA) that target human BTK mRNA.[31] Similarly, Heinonen et al. reported LFM-A13 and BTK-specific siRNA duplexes have virtually identical biological effects on mast cells.[32] Glassford et al. reported that the B-cell receptor signaling responses of LFM-A13 treated B-cells closely mimic those of B-cells from BTK-deficient mice.[33] Feldhahn et al. reported that LFM-A13 abrogates calcium signaling in pre-B ALL cells.[34] Fernandes et al. reported that LFM-A13 inhibits not only BTK but the other member of the TEC kinase family, TEC, as well.[35]

In accordance with the anti-apoptotic function of BTK, LFM-A13 disrupted BTK-Fas association and rendered resistant leukemic cells sensitive to Fas-mediated apoptosis.[30,39] In accordance with the anti-apoptotic function of BTK, treatment of BTK^+ B-lineage leukemia cells, including pre-B ALL cells and BCR-ABL+ pre-pre-B ALL cells, with LFM-A13 enhanced their sensitivity to vincristine- and ceramide-induced apoptosis.[39,30] Therefore, LFM-A13 shows potential as an anti-leukemic agent with apoptosis-promoting and chemosensitizing properties.

The potential of LFM-A13 as a chemosensitizing anti-leukemic agent was further explored in BALB/c mice challenged with chemotherapy-resistant BCL-1 B-lineage leukemia cells. In this model, 100% of mice die within 3 weeks after i.v. inoculation of 1×10^6 BCL-1 cells with a median survival of 13.5 days. LFM-A13 was not toxic to mice when administered systemically at dose levels ranging from 1 mg/kg to 100 mg/kg. Highly effective BTK-inhibitory and apoptosis-promoting plasma concentrations of LFM-A13 could be achieved in mice without any significant toxicity associated with morbidity or mortality.[28] LFM-A13 significantly improved the chemotherapy response and survival outcome of mice challenged with BCL-1 leukemia cells.[28] These results provided the foundation for the development of LFM-A13 as a new chemosensitizing and apoptosis-promoting antileukemic agent. LFM-A13 may potentiate the anti-leukemic effect of the individual components of induction chemotherapy as well as post-induction intensification and maintenance chemotherapy by inhibiting the BTK-dependent anti-apoptotic chemotherapy resistance of leukemic cells. Therefore, LFM-A13 may be clinically useful when used as part of remission–induction therapy, intensification (or consolidation) therapy as well as maintenance therapy to eliminate residual leukemia. The contribution of the previously unknown Plk-inhibitory activity of LFM-A13 to its anti-leukemic activity is unknown.

In summary, we discovered that LFM-A13, a rationally designed inhibitor of BTK tyrosine kinase, is a potent inhibitor of Plk and exhibits anti-proliferative activity against breast cancer cells both in vitro and in vivo. This study confirms and extends recent work with other small molecule inhibitors of Plk.[36,37] Scytonemin inhibits PLK at micromolar concentrations but it also inhibits multiple other kinases, including CDK1, CHK1, MYT, and PKC.[36,37] The dihydropteridinone BI-2536 also inhibits PLK and exhibits in vitro as well as in vivo antiproliferative activity and is currently being examined for toxicity in Phase I clinical trials.[36,37] ON01910, which is in clinical development, is an inhibitor of multiple kinases, including PLK, and induces apoptosis at micromolar concentrations.[36,37] By comparison, LFM-A13 appears to be more selective in its inhibitory activity profile against serine/threonine kinases and it does not induce apoptosis in human cancer cells. Notably, none of the 7 non-Plk serine/threonine kinases, including CDK-1, 2, -3, CHK1, IKK, MAPK1, and SAPK2a, was inhibited by LFM-A13. As better antibodies to specific members of the Plk kinase family become available and as

Table 2. Effects of LFM-A13 on peripheral blood counts in mice

Parameters	Vehicle ($n = 20$)	LFM-A13 (mg/kg)			
		80 ($n = 20$)	40 ($n = 20$)	20 ($n = 20$)	10 ($n = 20$)
Day 7 evaluation of acute toxicity					
Hematology					
WBC ($\times 10^9$/L)	6.5 ± 0.4	6.6 ± 0.5	7.0 ± 0.5	7.6 ± 0.6	7.0 ± 0.5
ANC ($\times 10^9$/L)	1.3 ± 0.1	1.7 ± 0.1	1.6 ± 0.2	1.4 ± 0.2	1.3 ± 0.1
ALC ($\times 10^9$/L)	4.9 ± 0.3	4.6 ± 0.4	5.2 ± 0.4	5.8 ± 0.5	5.4 ± 0.4
Bone/Bone marrow					
Within normal limits	20/20	20/20	20/20	20/20	19/20
Myeloid or lymphoid hypoplasia	0/20	0/20	0/20	0/20	0/20
Day 30 evaluation of subacute toxicity					
Hematology					
WBC ($\times 10^9$/L)	6.0 ± 0.5	6.1 ± 0.5	6.4 ± 0.4	6.2 ± 0.5	6.0 ± 0.4
ANC ($\times 10^9$/L)	1 ± 0.1	1.7 ± 0.1	1 ± 0.1	2.2 ± 0.2	1.4 ± 0.2
ALC ($\times 10^9$/L)	4.7 ± 0.4	4.3 ± 0.4	5.1 ± 0.4	3.9 ± 0.4	4.4 ± 0.3
Bone/Bone marrow					
Within normal limits	19/20	20/20	20/20	19/20	20/20
Myeloid or lymphoid hypoplasia	0/20	0/20	0/20	0/20	0/20

CD-1 mice were treated with an ip bolus injection of LFM-A13 at the indicated dose levels. Mice were electively sacrificed on day 7 or 30. Laboratory results are presented as means ± SEM values of laboratory parameters for each dose level. At death, femurs were collected and processed for histologic bone marrow examinations. The histology slides were stained with hematoxylin and eosin.

Table 3. Effects of LFM-A13 on peripheral blood counts in rats

Parameters	Vehicle ($n = 10$)	LFM-A13 (mg/kg)		
		80 ($n = 10$)	40 ($n = 10$)	20 ($n = 10$)
Hematology				
WBC ($\times 10^9$/L)	11.9 ± 1.0	11.7 ± 0.9	12.9 ± 0.5	11.7 ± 0.7
ANC ($\times 10^9$/L)	1.8 ± 0.0	1.8 ± 0.0	2.1 ± 0.0	1.6 ± 0.0
ALC ($\times 10^9$/L)	9.9 ± 0.0	9.7 ± 0.0	10.6 ± 0.0	9.8 ± 0.0
Bone/Bone marrow				
Within normal limits	10/10	10/10	10/10	10/10
Myeloid or lymphoid hypoplasia	0/10	0/10	0/10	0/10

Lewis rats were treated with an iv bolus injection of LFM-A13 at the indicated dose levels. Rats were electively sacrificed on day 7. Laboratory results are presented as means ± SEM values of laboratory parameters for each daily dose level. At death, femurs were collected, and processed for histologic bone marrow examination. The histology slides were stained with hematoxylin and eosin.

Table 4. Effects of LFM-A13 on non-proliferating tissues in mice and rats

Animal	LD_{10}[b] (mg/kg)	Toxic organ lesions[c]			
		Kidney	Lung	Brain	Myocardium
CD-1 mice ($N = 160$)	>80 (ip)	—	—	—	—
Lewis rats ($N = 30$)	>80 (iv)	—	—	—	—
BALB/c mice ($N = 75$)	>100 (po)	—	—	—	—
BALB/c mice ($N = 80$)[a]	>200 (daily po)	—	—	—	—
	>11,200 (cumulative po)				

[a] In this experiment BALB/c mice were treated with 100 or 200 mg/kg LFM-A13 daily for 7–56 consecutive days.
[b] LD10 (lethal dose that kills 10% of animals) values are expressed for the daily dose as well as the cumulative dose.
[c] At death, mice and rats had postmortem examinations. Selected tissues were collected, fixed in 10% formalin, and processed for histologic sectioning. The histology slides were stained with hematoxylin and eosin.

we learn more about their specific downstream substrates, it will be interesting to evaluate the effects of LFM-A13 on the phosphorylation of such substrates by the specific Plk kinases in normal and malignant cells at different phases of the cell cycle. The remarkable in vivo activity and safety profile of LFM-A13 warrants the further development of this promising new anti-cancer agent for possible clinical use in cancer patients.

4. Materials and methods

4.1. Construction of a homology model for the kinase domain of Plx1

We have constructed a homology model of the *Xenopus* Plk homolog Plx1[7,38] using the X-crystal structure of cAMP-dependent protein kinase since no experimentally

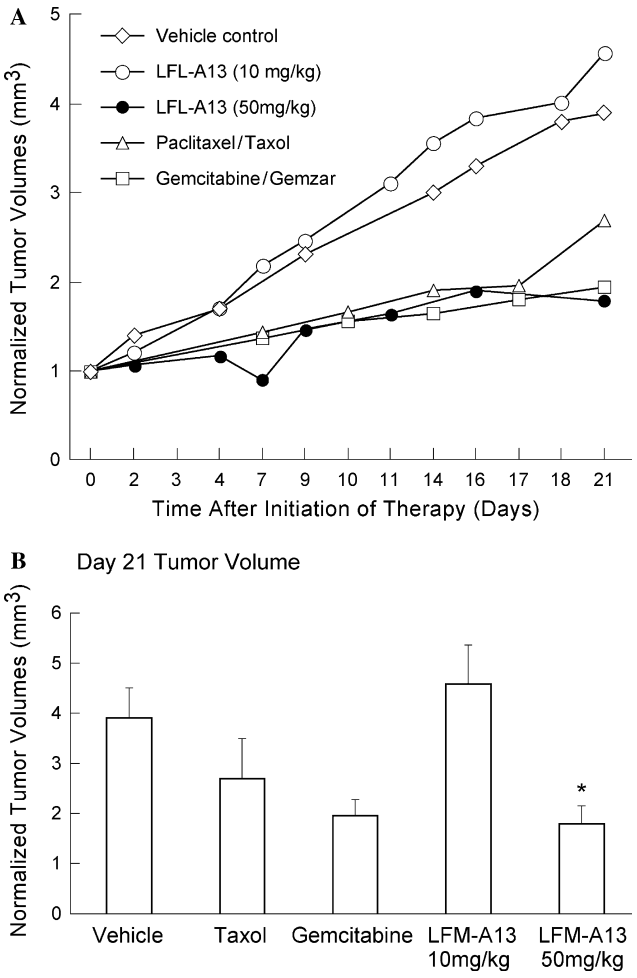

Figure 8. Effects of LFM-A13 on tumor progression in MMTV/*Neu* transgenic mice. Tumor growth was determined by the measurement of tumors with a caliper in three dimensions three days a week and expressed as tumor volume in cubic millimeters (mm^3). Tumor volumes were calculated using the formula for the volume of a prolate spheroid, $V = 4/3 \times 3.14 \times \text{length}/2 \times \text{width}/2 \times \text{depth}/2$. Tumor growth for each mouse was normalized to the starting volume for that particular tumor. Therefore, each mouse also served as its own control, and the tumor growth curves were generated to show the rate of change in tumor volumes. LFM-A13 (10 or 50 mg/kg) was administered by twice daily intraperitoneal injections on 5 consecutive days per week. Paclitaxel was administered intraperitoneally on days 1, 3, 5, 8, 10, and 12 at a dose level of 6.7 mg/kg. Gemcitabine was administered on days 1, 8, and 15 at a dose level of 33.7 mg/kg. $^*P < 0.05$, Linear contrast versus vehicle.

determined three-dimensional coordinates have been reported for the Plx1-KD. The homology modeling of the Plx1-KD was carried out by first obtaining the protein sequence alignment using the homology module within InsightII program suite.[39] Next, a set of three-dimensional coordinates was assigned to the Plx1 sequence using the coordinates of cAMP protein kinase as a template, which employed the homology module. The coordinates for a loop region where a sequence insertion occurs (relative to cAMP without the loop) were chosen from a limited number of possibilities automatically generated by the program and manually adjusted to a more ideal geometry using the program CHAIN. Finally, the constructed model of Plx1-KD was subjected to energy minimization using the X-PLOR program so that any steric strain introduced during the model-building process could be relieved. The model was screened for unfavorable steric contacts, and if necessary such side chains were remodeled either by using a rotamer library database or by manually rotating the respective side chains. The final homology model of Plx1-KD was then used, in conjunction with model coordinates of LFM-A13 for our modeling studies of the Plx1-KD/LFM-A13 complex.

4.2. Molecular modeling studies

Modeling of leflunomide metabolite (LFM) analogs with Plx1-KD was accomplished using the docking module within the program INSIGHTII[39] and using the affinity suite of programs for automatically docking an inhibitor into a protein binding site. The starting positions in the docking procedure were chosen on the basis of a favorable fit into the binding site and/or favorable hydrogen bonding interactions between the inhibitor and binding site residues. Because LFM compounds have only one suitable hydrogen bond forming site with the Cys-124 amide, the initial positions were selected with ease by placing the cyano group of the molecule within 3.5 Å away from the amide group and without major steric clash with surrounding residues. The initial coordinates of LFM compounds were either directly taken from X-ray structure of leflunomide or small modification of it. The initial positions as a rigid body were also changed automatically and sampled randomly in the subsequent Monte Carlo simulation and docking calculation. The docking method in the InsightII program used the CVFF force field and a Monte Carlo search strategy to search for and evaluate docked structures. While the coordinates for the bulk of the receptor were kept fixed, a defined region of the binding site was allowed to relax, thereby allowing the protein to adjust to the binding of different inhibitors. A binding set was defined with 7 Å from the inhibitor, allowing residues within this distance to shift and/or rotate to energetically favorable positions to accommodate the ligand. An assembly was defined consisting of the receptor and inhibitor molecule, and docking was performed using the fixed docking mode. Calculations approximating hydrophobic and hydrophilic interactions were used to determine the 10 best docking positions of each LFM compound in the Plx1-KD catalytic site. The various docked positions of each compound were evaluated using a Ludi scoring procedure in INSIGHTII[39] which estimated a binding constant, K_i, taking into account the predicted lipophilic, hydrogen bonding, and van der Waals interactions between the inhibitor and the protein. The resulting orientation that gave the best docking score for LFM-A13 is shown in Figure 1.

4.3. Recombinant Plx1 protein

Sf21 (IPLB-SF21-AE) cells,[39] derived from the ovarian tissue of the fall armyworm *Spodoptera frugiperda*, were obtained from Invitrogen and maintained at 26–28 °C in Grace's insect cell medium supplemented with 10% fetal bovine serum and 1.0% antibiotic/antimycotic (Life

Technologies, Inc.). Stock cells were maintained in suspension at 0.2–1.6 × 10^6/ml in 600-ml total culture volume in 1-L Bellco spinner flasks at 60–90 rpm. Cell viability was maintained at 95–100% as determined by trypan blue dye exclusion. Construction of the recombinant baculovirus expression vector containing the gene for Plx1, the *Xenopus* homolog of Plk, was previously reported.[7] 60 × 10^6 Sf21 cells were transfected with recombinant His6-Plx1 expression vector encoding the full-length *Xenopus* Plx1 protein fused to six tandem repeats of histidine residues at the N-terminus of the protein with the standard liposome-mediated method using Cellfectin reagent (Life Technologies, Inc.). Forty-six hours post-transfection, Sf21 cells were treated with 100 nM okadaic acid (Life Technologies). Three hours post treatment with okadaic acid, the cells were harvested, lysed using the same lysis buffer previously reported,[7] and recombinant His6-Plx1 was purified using nickel agarose gel chromatography.[7] The purity of each preparation was measured by SDS–PAGE followed by Coomassie blue staining. The activity of purified Plx1 was measured by autophosphorylation in the presence of [γ-^{32}P]ATP. GST-Cdc25 (254–316) fusion protein containing amino acids 254-316 of the wildtype *Xenopus* Cdc25 was prepared as previously described.[40]

4.4. Intrinsic protein fluorescence quenching measurements

Tryptophan (Trp) residues of proteins contribute to their intrinsic fluorescence. Changes in intrinsic fluorescence can be used to monitor conformational changes in a protein that occur after ligand binding. A Beckman DU 650 spectrophotometer was used to measure absorption spectra. Fluorescence was measured by means of a Shimadzu 5301 PC spectrofluorometer controlled by a data system station. Protein fluorescence was excited at 295 nm to minimize the contribution of protein tyrosine residues to the intrinsic fluorescence. Changes in protein fluorescence were monitored at 340 nm. The slit widths on both the excitation and emission monochromators were set at 2.5 nm. The sample department of the instrument was maintained at 20 °C with a circulating water bath. The binding of LFM-A13 to purified Plx1 was studied by measuring the intrinsic fluorescence intensity of Plx1 protein in the presence and absence of increasing concentrations of LFM-A13 to determine the magnitude of LFM-A13-mediated quenching of intrinsic Trp fluorescence and the data were analyzed as previously reported.[41,42]

4.5. Kinase assays

LFM-A13 was prepared as previously reported.[39] Purified His6-Plx1 (250 ng) was added to a 20 μL reaction mixture containing 1× kinase buffer (10 mM Tris–HCl, pH 7.5, 10 mM $MgCl_2$, and 1 mM TT), 25 μM cold ATP, and 1 μCi [γ-^{32}P]ATP in the presence of different concentrations of LFM-A13 ranging from 5 μg/mL (13.9 μM) to 100 μg/mL (278 μM). The reaction mixtures were incubated at room temperature for 15–30 min and autophosphorylation was stopped by addition of 2× SDS–PAGE reducing sample buffer. A parallel experiment was performed in the presence of cold ATP. The kinase reactions were then subjected to immunoblotting using the commercially available anti-Plk antibodies. The immunoblots confirmed that the same amount of Plx1 protein was present in each reaction. In addition, we also examined the effects of LFM-A13 on substrate phosphorylation by Plx1. In brief, 250 ng of purified Plx1 was first incubated at room temperature for one hour with different concentrations of LFM-A13. After one hour of incubation, the tubes containing the reaction mixtures were put on ice and the substrate, GST-Cdc25 peptide (254–316) (200 ng), kinase buffer, and [γ-^{32}P]ATP were added and the kinase reaction allowed to proceed for 15 min at room temperature. Immunoblotting with anti-Cdc25 antibodies was used to confirm that equal amounts of the substrate peptide were present in each reaction mixture. Anti-Plk antibodies were obtained from Zymed Laboratories Inc (San Francisco, CA). The polyclonal antibodies to gluthathione-*S*-transferase (GST) were obtained from Upstate Biotechnology (Lake Placid, NY). ECL kit was obtained from Millipore Corp (Bedford, MA). The mode of human PLK3 inhibition by LFM-A13 was examined in titration experiments using increasing concentrations of [γ-^{32}P]ATP and purified N-terminal His6-tagged recombinant human PLK3, residues 19–301, expressed by baculovirus in Sf21 insect cells. In brief, in a final reaction volume of 25 μl, PLK3 (h) (5–10 mU) was incubated with 8 mM MOPS, pH 7.0, 0.2 mM EDTA, 2 mg/ml casein, 10 mM Mg acetate, and [γ-^{32}P-ATP] (specific activity approx. 500 cpm/pmol, concentration as required). The reaction was initiated by the addition of the MgATP mix. After incubation for 40 min at room temperature, the reaction was stopped by the addition of 5 μl of a 3% phosphoric acid solution. Ten microliters of the reaction was then spotted onto a P30 filtermat and washed three times for 5 min in 75 mM phosphoric acid and once in methanol prior to drying and scintillation counting. The K_i of PLK3 by LFM-A13 was calculated from the reciprocal plots of the intensity of phosphorylation of the substrate ($1/v$) versus the concentration of the inhibitor (i) (viz., LFM-A13). From this Dixon plot, the K_i represents the dissociation constants of the EI complex, which is determined by the point of linear intersection.[43,44] The specificity of LFM-A13 was further examined against a broad panel of serine/threonine kinases, tyrosine kinases, and one lipid kinase using the KinaseProfilerTM Assay protocols from Upstate (Charlottesville, Virginia).

To calculate the IC_{50} value for LFM-A13 against each of the protein kinases, an iterative nonlinear regression method using least-squares was used to fit the dose effect equation. % Inhibition = $(100 \times [\text{LFM-A13}])/(IC_{50})/(100 + [\text{LFM-A13}]/IC_{50})$. The convergence to a solution employed a Gauss–Newton method with a line search. This method uses derivatives of the model with respect to the IC_{50} parameter and the parameter value with the least sum of squares (square of data minus model calculated value) resulted in the IC_{50} determination. To calculate the K_i value, the IC_{50} values for concentration-dependent inhibition of PLK3 by LFM-A13 using

the dose effect equation at each ATP concentration. Plk-kinase activity inhibited by LFM-A13 were calculated (25, 100, 200 μM) at 5 ATP concentrations (25, 50, 75, 100, 200 μM) was fitted using linear regression to the Cheng–Prusoff equation:[45] $IC_{50} = K_i/K_m \times [ATP] + K_i$. K_i was determined directly from the intercept of the plot of [ATP] versus IC_{50} values.

4.6. Zebrafish drug-screening assay

The adult wild-type zebrafish (obtained from Blaine Fish Co., Minneapolis, MN) were maintained according to previously described methods.[26,27] For water-borne drug administration the zebrafish eggs were removed from chorions by mild digestion in 1% Trypsin–EDTA (Sigma, St Louis, MO) for 10 min at 28.5 °C (standard temperature—ST), washed three times with 'egg water' and twice with embryo medium (EM).[26,27] The dechorionated two-cell stage cleaving eggs were transferred to 24-well plastic cell culture plates (Corning Costar, Acton, MA) filled with EM. The eggs (10–12 per well) were exposed to the drug at a constant ST for 3 h. The final volume of the medium in each well was 500 μL. The compounds were used at concentrations ranging from 10 μM to 1 mM. They were dissolved initially in dimethylsulfoxide (DMSO, Sigma, St. Louis, MO) used as a drug carrier and then diluted serially with the incubation medium. The final concentration of DMSO in the wells did not exceed the damaging concentration of above 3%. The sham-treated control embryos were incubated in EM in the presence of 3% DMSO. Observations of cell division and development of the zebrafish eggs were carried out using an SMZ-10A stereo microscope (Nikon Inc., Melville, NY) once every 15 min within the first six hours of incubation. The drug effect was considered to be revealed when all the eggs from one well were affected in the same characteristic manner in three independent experiments. The stereomicroscope was fitted with a specially designed transparent heating tray in order to keep embryos at ST during observations. Pictures of the eggs and embryos were taken with an H-III Photomicrographic System (Nikon Inc., Melville, NY) using Ektachrome 64X film (Kodak, Rochester, NY).

4.7. Microinjection and time-lapse imaging

PTK1, a rat kangaroo (*Potorous tridactylis*) epithelial cell line, was used in microinjection experiments. PTK1 cells were plated on poly-L-lysine-coated, glass-bottomed, 35 mm Petri dishes (Mattek Corp., Ashland, MA) and grown in minimal essential medium (MEM) supplemented with 10% fetal bovine serum (FBS) for 24 h. Randomly selected premitotic cells were injected with 100 μM LFM-A13 using an Eppendorf system (Transjector 5246) under an inverted phase microscope. Cells were imaged for an hour in 1-min intervals using a Nikon Diaphot 200 inverted phase microscope mounted with a stage-top incubator in which the temperature was kept at 37 °C. Digital images were saved using the Metamorph 4.0 software (Universal Imaging Corp) and later processed with Adobe Photoshop software (Adobe Systems, Mountain View, CA).

4.8. Confocal laser scanning microscopy

Immunofluorescence and confocal microscopy[26,27] were used to examine the spindle features of BT-20 human breast cancer cell line and U373 human glioblastoma cell line treated with LFM-A13 (100 μM) or 0.5% DMSO. Initially, cells at log phase were seeded onto sterile 22 mm coverslips in six-well culture plates. Twenty-four hours later, the cells were treated with LFM-A13 (100 μM) for 2 h at 37 °C, 5% CO_2, fixed in methanol (−20 °C, 15 min) followed by a 15 min incubation with PBS + 0.1% TX-100. The cells were then stained for α-tubulin as well as γ-tubulin. Cellular DNA was also labeled with 5 μM TOTO3 (Molecular Probes, Eugene, OR). Coverslips were immediately inverted onto slides in Vectashield (Vector Labs, Burlingame, CA) to prevent photobleaching, sealed with nail varnish, and stored at −20 °C. The slides were examined using a Bio-Rad MRC-1024 Laser Scanning Confocal Microscope equipped with a Kr/Ar laser (Bio-Rad, Hercules, CA) mounted on a Nikon Eclipse E800 upright microscope with high numerical aperture objectives (Nikon, Melville, NY). Digital data were processed using Lasersharp (BioRad) and Adobe Photoshop software (Adobe Systems, Mountain View, CA).

4.9. Animals for toxicity evaluations

CD-1 mice and BALB/c mice (Charles River, Willmington, MA) were housed in microisolator cages (Lab Products, Inc., Maywood, NY) in a controlled USDA-accredited environment (12-h light/12-h dark photoperiod, 22 ± 1 °C, 60 ± 10% relative humidity) under specific pathogen-free (SPF) conditions. Mice were allowed free access to autoclaved standard pellet food and tap water. Adult male Lewis rats (body weight: ~160 g) for rat toxicity studies were obtained from the SPF breeding facilities of Harlan Sprague–Dawley at 14 weeks of age. The animal studies were approved by the Parker Hughes Institute Animal Care and Use Committee. All animal care procedures conformed to the Guide for the Care and Use of Laboratory Animals (National Research Council, National Academy Press, Washington DC 1996).

4.10. Toxicity studies in mice

The toxicity profile of LFM-A13 in mice was examined, as previously reported.[28,29] In brief, mice were administered an intraperitoneal (i.p.) bolus injection of LFM-A13 in 0.2 mL PBS supplemented with 10% DMSO, or 0.2 mL PBS supplemented with 10% DMSO alone (control mice). In other studies, mice were treated with oral doses of LFM-A13 via gavage. No sedation or anesthesia was used throughout the treatment period. Mice were monitored daily for mortality for determination of the day 30 LD_{10} values. Blood counts (red blood cells [RBC], white blood cells [WBC], and platelets [Plt]) were determined using a HESKA Vet ABC-Diff Hematology Analyzer (HESKA Corporation, Fort Collins, CO, USA). Absolute neutrophil counts (ANC) and absolute lymphocyte counts (ALC) were calculated from WBC values after determining the percentages of neutrophils and lymphocytes by a manual differential count.

Values for the laboratory parameters were pooled for vehicle controls and LFM-A13 treatments, and for each parameter differences between means were evaluated for statistical significance using Student's *t*-test (vehicle vs LFM-A13 treatment, unequal variances, two-tailed). The calculations were performed in Excel spreadsheets. To determine significant effects, the *p*-values were adjusted using the Bonferroni method to control for random variation. Mice surviving until the end of the designated 1–8 week monitoring period were sacrificed and several tissues were immediately collected for histopathologic examination. For histopathologic studies, tissues were fixed in 10% neutral buffered formalin, dehydrated, and embedded in paraffin by routine methods. Glass slides with affixed 6 micron tissue sections were prepared and stained with hematoxylin and eosin (H&E).

4.11. Toxicity studies in rats

Lewis rats were kept in microisolater cages (Allentown Caging Equipment Co., Inc., Allentown, NJ, USA) containing autoclaved food, water, and bedding. All husbandry and experimental contact made with the mice and rats maintained SPF conditions. Animal studies were approved by Parker Hughes Institute Animal Care and Use Committee and all animal care procedures conformed to the Guide for the Care and Use of Laboratory Animals (National Research Council, National Academy Press, Washington, DC 1996, USA). Lewis rats were treated with i.v. injections of LFM-A13 at multiple dose levels. LFM-A13 was administered as a 0.5 mL bolus injection containing 10% DMSO as a vehicle. Animals were electively sacrificed on day 7 to determine the toxicity of LFM-A13 by evaluating multiple organs for the presence of toxic lesions. Blood was collected by intracardiac puncture following anesthesia with ketamine:xylazine and immediately heparinized. Blood counts (red blood cells [RBC], white blood cells [WBC], and platelets [Plt]) were determined using a HESKA Vet ABC-Diff Hematology Analyzer (HESKA Corporation, Fort Collins, CO, USA). Absolute neutrophil counts (ANC) and absolute lymphocyte counts (ALC) were calculated from WBC values after determining the percentages of neutrophils and lymphocytes by a manual differential count. Values for the laboratory parameters were pooled for vehicle controls and LFM-A13 treatments, and for each parameter differences between means were evaluated for statistical significance using Students *t*-test (vehicle vs LFM-A13 treatment, unequal variances, two-tailed). The calculations were performed in Excel spreadsheets. To determine significant effects, the *p*-values were adjusted using the Bonferroni method to control for random variation. For histopathologic studies, formalin fixed tissues were dehydrated and embedded in paraffin by routine methods. Glass slides with affixed 4–5 micron tissue sections were prepared and stained with hematoxylin and eosin (H&E).

4.12. MMTV/*Neu* transgenic mice

Overexpression of the wild type *Neu* in the mammary glands of transgenic mice induces metastatic breast cancer.[26] Accordingly, in the MMTV/*Neu* transgenic strain, the wildtype *neu* is overexpressed in the mammary gland under the control of the MMTV long terminal repeat. This animal model has been used to analyze the Her2/*neu* overexpression in breast epithelia, as well as the efficacy of new therapeutic approaches to prevent or treat Her2/*Neu* overexpressing malignancies. MMTV/*Neu* mice [FVB/N-TgN(MMTV/*neu*)202MUL; Jackson Laboratory, Bar Harbor, Maine] were bred to produce multiple litters in a controlled SPF envirnoment (12 h light/12 h-dark photoperiod, 22 ± 1 °C, $60 \pm 10\%$ relative humidity), which is fully accredited by the United States Department of Agriculture.

The genotype of mice was confirmed by multiplex polymerase chain reaction (PCR) tests, as described.[26] *Neu* transgenic mice carrying one or more tumors were randomly placed in the study. For the evaluation of tumor kinetics, tumor-bearing mice were randomly assigned to either vehicle control or treatment groups. Tumor growth was determined by the measurement of tumors with a caliper in three dimensions three days a week and expressed as tumor volume in cubic millimeters (mm^3). Tumor volumes were calculated using the formula for the volume of a prolate spheroid, $V = 4/3 \times 3.14 \times \text{length}/2 \times \text{width}/2 \times \text{depth}/2$. Due to the large heterogeneity in transgenic tumor volumes on day 0, tumor growth for each mouse was normalized to the starting volume for that particular tumor. Therefore, each mouse also served as its own control, and the tumor growth curves were generated to show the rate of change in tumor volumes. LFM-A13 (10 or 50 mg/kg) was administered by twice daily intraperitoneal injections on 5 consecutive days per week. Paclitaxel was administered intraperitoneally on days 1, 3, 5, 8, 10, and 12 at a dose level of 6.7 mg/kg. Gemcitabine was administered on days 1, 8, and 15 at a dose level of 33.7 mg/kg. Paclitaxel and gemcitabine were obtained from Parker Hughes Cancer Center Pharmacy.

4.13. Statistical methods for tumor progression

Normalized tumor volumes (log 10 transformed to homogenize group variances) were measured over 21 days. Multivariate analysis of variance (MANOVA) model was constructed to measure the overall effect of drug treatment (Vehicle control, Taxol, Gemcitabine, LFM-A13 50 mg/kg, LFM-A13 10 mg/kg) across three time points: 7, 14, and 21 days. The MANOVA controlled for starting volume (tumor volumes at day zero); treatment effect, and starting volume × treatment interactions were assessed for significance using exact *F*-statistics ($p < 0.05$ deemed significant). In an attempt to determine at which time points the treatment effect occurred, an analysis of co-variance (ANCOVA) model was constructed and used to measure the effect sizes of drug treatment controlling for start volume at days 7, 14 and 21. In this model, the treatment group was the fixed effect, the start volume was the covariate and an interaction term was included to determine the significance of the start volume on the treatment effect. We used linear contrasts to determine the effect of each drug treatment relative to the vehicle control at each day of

measurement. Contrasts are constructed such that the combination of linear parameters to be jointly tested sum to zero for each level of the contrast. In our design, least square mean values were used to construct contrasts between each of the drug treatments (set to −1) and vehicle control (set to 1). All calculations were performed using JMP software (Cary, NC). Linear Contrasts included the following: LFM-A13 50 mg/kg versus Vehicle; LFM-A13 10 mg/kg versus Vehicle; Paclitaxel versus Vehicle; Gemcitabine versus Vehicle; LFM-A13 50 mg/kg versus Gemcitabine, Paclitaxel. Multivariate analysis of variance (MANOVA) model was constructed to measure the overall effect of treatment on the size and growth of multiple target tumors in vehicle control ($n = 8$ mice), Paclitaxel ($n = 6$ mice), Gemcitabine ($n = 7$ mice), LFM-A13, 50 mg/kg ($n = 5$ mice), and LFM-A13, 10 mg/kg ($n = 6$ mice) treatment groups.

References and notes

1. Donaldson, M. M.; Tavares, A. A.; Hagan, I. M.; Nigg, E. A.; Glover, D. M. *J. Cell Sci.* **2001**, *114*, 2357–2358.
2. Glover, D. M.; Hagan, I. M.; Tavares, A. A. *Genes Dev.* **1998**, *12*, 3777–3787.
3. Nigg, E. A. *Curr. Opin. Cell Biol.* **1998**, *10*, 776–783.
4. Roshak, A. K.; Capper, E. A.; Imburgia, C.; Fornwald, J.; Scott, G.; Marshall, L. A. *Cell. Signal.* **2000**, *12*, 405–411.
5. Abrieu, A.; Brassac, T.; Galas, S.; Fisher, D.; Labbe, J. C.; Doree, M. *J. Cell Sci.* **1998**, *111*, 1751–1757.
6. Descombes, P.; Nigg, E. A. *EMBO J.* **1998**, *17*, 1328–1335.
7. Kumagai, A.; Dunphy, W. G. *Science* **1996**, *273*, 1377–1380.
8. Song, S.; Grenfell, T. Z.; Garfield, S.; Erikson, R. L.; Lee, K. S. *Mol. Cell. Biol.* **2000**, *20*, 286–298.
9. Lee, K. S.; Erikson, R. L. *Mol. Cell. Biol.* **1997**, *17*, 3408–3417.
10. Knecht, R.; Elez, R.; Oechler, M.; Solbach, C.; von Ilberg, C.; Strebhardt, K. *Cancer Res.* **1999**, *59*, 2794–2797.
11. Strebhardt, K.; Kneisel, L.; Linhart, C.; Bernd, A.; Kaufmann, R. *JAMA* **2000**, *283*, 479–480.
12. Takai, N.; Miyazaki, T.; Fujisawa, K.; Nasu, K.; Hamanaka, R.; Miyakawa, I. *Cancer Lett.* **2001**, *164*, 41–49.
13. Tokumitsu, Y.; Mori, M.; Tanaka, S.; Akazawa, K.; Nakano, S.; Niho, Y. *Int. J. Oncol.* **1999**, *15*, 687–692.
14. Wolf, G.; Elez, R.; Doermer, A.; Holtrich, U.; Ackermann, H.; Stutte, H. J.; Altmannsberger, H. M.; Rubsamen-Waigmann, H.; Strebhardt, K. *Oncogene* **1997**, *14*, 543–549.
15. Kanaji, S.; Saito, H.; Tsujitani, S.; Matsumoto, S.; Tatebe, S.; Kondo, A.; Ozaki, M.; Ito, H.; Ikeguchi, M. *Oncology* **2006**, *70*, 126–133.
16. Reagan-Shaw, S.; Ahmad, N. *IUBMB Life* **2005**, *57*, 677–682.
17. Spankuch-Schmitt, B.; Wolf, G.; Solbach, C.; Loibl, S.; Knecht, R.; Stegmuller, M.; von Minckwitz, G.; Kaufmann, M.; Strebhardt, K. *Oncogene* **2002**, *21*, 3162–3171.
18. Weichert, W.; Kristiansen, G.; Winzer, K. J.; Schmidt, M.; Gekeler, V.; Noske, A.; Muller, B. M.; Niesporek, S.; Dietel, M.; Denkert, C. *Virchows Arch.* **2005**, *446*, 442–450.
19. Spankuch, B.; Heim, S.; Kurunci-Csacsko, E.; Lindenau, C.; Yuan, J.; Kaufmann, M.; Strebhardt, K. *Cancer Res.* **2006**, *66*, 5836–5846.
20. Cogswell, J. P.; Brown, C. E.; Bisi, J. E.; Neill, S. D. *Cell Growth Differ.* **2000**, *11*, 615–623.
21. Liu, X.; Erikson, R. L. *Proc. Natl. Acad. Sci. U.S.A.* **2003**, *100*, 5789–5794.
22. Ahmad, N. *FASEB J.* **2004**, *18*, 5–7.
23. Lane, H. A.; Nigg, E. A. *J. Cell Biol.* **1996**, *135*, 1701–1713.
24. Spankuch-Schmitt, B.; Bereiter-Hahn, J.; Kaufmann, M.; Strebhardt, K. *J. Natl. Cancer Inst.* **2002**, *94*, 1863–1877.
25. Spankuch, B.; Matthess, Y.; Knecht, R.; Zimmer, B.; Kaufmann, M.; Strebhardt, K. *J. Natl. Cancer Inst.* **2004**, *96*, 862–872.
26. Uckun, F. M.; Vassilev, A. O.; Dibirdik, I.; Liu, X. P.; Erbeck, D.; Tibbles, H. E.; Qazi, S.; Venkatachalam, T. K. *Arzneimittelforschung* **2004**, *54*, 715–731.
27. Navara, C. S.; Benyumov, A.; Vassilev, A.; Narla, R. K.; Ghosh, P.; Uckun, F. M. *Anticancer Drugs* **2001**, *12*, 369–376.
28. Uckun, F. M.; Zheng, Y.; Cetkovic-Cvrlje, M.; Vassilev, A.; Lisowski, E.; Waurzyniak, B.; Chen, H.; Carpenter, R.; Chen, C. L. *Clin. Cancer Res.* **2002**, *8*, 1224–1233.
29. Tibbles, H. E.; Samuel, P.; Erbeck, D.; Mahajan, S.; Uckun, F. M. *Arzneimittelforschung* **2004**, *54*, 330–339.
30. Vassilev, A.; Ozer, Z.; Navara, C.; Mahajan, S.; Uckun, F. M. *J. Biol. Chem.* **1999**, *274*, 1646–1656.
31. Kim, Y. J.; Sekiya, F.; Poulin, B.; Bae, Y. S.; Rhee, S. G. *Mol. Cell. Biol.* **2004**, *24*, 9986–9999.
32. Heinonen, J. E.; Smith, C. I.; Nore, B. F. *FEBS Lett.* **2002**, *527*, 274–278.
33. Glassford, J.; Soeiro, I.; Skarell, S. M.; Banerji, L.; Holman, M.; Klaus, G. G.; Kadowaki, T.; Koyasu, S.; Lam, E. W. *Oncogene* **2003**, *22*, 2248–2259.
34. Feldhahn, N.; Rio, P.; Soh, B. N.; Liedtke, S.; Sprangers, M.; Klein, F.; Wernet, P.; Jumaa, H.; Hofmann, W. K.; Hanenberg, H.; Rowley, J. D.; Muschen, M. *Proc. Natl. Acad. Sci. U.S.A.* **2005**, *102*, 13266–13271.
35. Fernandes, M. J.; Lachance, G.; Pare, G.; Rollet-Labelle, E.; Naccache, P. H. *J. Leukocyte Biol.* **2005**, *78*, 524–532.
36. McInnes, C.; Mezna, M.; Fischer, P. M. *Curr. Top. Med. Chem.* **2005**, *5*, 181–197.
37. Strebhardt, K.; Ullrich, A. *Nat. Rev. Cancer* **2006**, *6*, 321–330.
38. Kelm, O.; Wind, M.; Lehmann, W. D.; Nigg, E. A. *J. Biol. Chem.* **2002**, *277*, 25247–25256.
39. Mahajan, S.; Ghosh, S.; Sudbeck, E. A.; Zheng, Y.; Downs, S.; Hupke, M.; Uckun, F. M. *J. Biol. Chem.* **1999**, *274*, 9587–9599.
40. Kumagai, A.; Guo, Z.; Emami, K. H.; Wang, S. X.; Dunphy, W. G. *J. Cell Biol.* **1998**, *142*, 1559–1569.
41. Appleman, J. R.; Lienhard, G. E. *J. Biol. Chem.* **1985**, *260*, 4575–4578.
42. Epps, D. E.; Raub, T. J.; Caiolfa, V.; Chiari, A.; Zamai, M. *J. Pharm. Pharmacol.* **1999**, *51*, 41–48.
43. Dixon, M. *Biochem. J.* **1953**, *55*, 170–171.
44. Tipton, K. F. In *Enzymology: LabFax*; Engel, P. C., Ed.; Academic Press: San Diego, CA, 1996; pp 115–121.
45. Cheng, Y.; Prusoff, W. H. *Biochem. Pharmacol.* **1973**, *2*, 3099–3108.